LAWRENCE
LIVERMORE
NATIONAL
LABORATORY

LLNL-JRNL-643494

A High-Pressure Rapid Compression Machine Study of n-Propylbenzene Ignition

D. Darcy, H. Nakamura, C. J. Tobin, M. Mehl, W. K. Metcalfe, W. J. Pitz, C. K. Westbrook, H. J. Curran

September 5, 2013

Combustion and Flame

Disclaimer

A High-Pressure Rapid Compression Machine Study of *n*-Propylbenzene Ignition

D. Darcy[a], H. Nakamura[a,b, 1], C.J. Tobin[a], M. Mehl[c], W.K. Metcalfe[a], W.J. Pitz[c], C.K. Westbrook[c], H.J. Curran[a]

[a]*Combustion Chemistry Centre, NUI Galway, Ireland*
[b]*Institute of Fluid Science, Tohoku University, 2-1-1 Katahira, Aoba-ku, Sendai, Miyagi 980-8577 Japan*
[c]*Lawrence Livermore National Laboratory, Livermore, CA 94551*

Abstract

This study presents new ignition delay data measured in a rapid compression machine over a wide range temperature, pressure and fuel/air ratio. This data is an extension of that measured previously (D. Darcy, C.J. Tobin, K. Yasunaga, J.M. Simmie, J. Würmel, T. Niass, O. Mathieu, S.S. Ahmed, C.K. Westbrook, H.J. Curran, Combust. Flame, 159 (2012) 2219–2232.) for the oxidation of *n*-propylbenzene in a high-pressure shock tube. The data was obtained for equivalence ratios of 0.29, 0.48, 0.96, and 1.92, at compressed gas pressures of 10, 30 and 50 atm, and over the temperature range of 650–1000 K. Experimental data was also obtained at 50 atm for all equivalence ratios in our new heated high-pressure shock tube and this is also presented here. Comparisons between the data obtained in both the rapid compression machine and the shock tube facilities showed excellent agreement. A previously published chemical kinetic mechanism has been improved and a low-temperature reaction mechanism has been added to simulate ignition delay times at the lower temperature conditions of this study by adding the appropriate species and reactions including alkyl-

[1] address: Institute of Fluid Science, Tohoku University, 2-1-1 Katahira, Aoba-ku, Sendai, Miyagi 980-8577, Japan. Phone: +81-22-217-5296. Email: nakamura@edyn.ifs.tohoku.ac.jp

Preprint submitted to Combustion and Flame May 15, 2013

peroxyl and hydroperoxy-alkyl radical chemistry. Special attention was given to $R\dot{O}_2$ isomerizations and $H\dot{O}_2$ elimination reactions involving the secondary benzylic site on *n*-propylbenzene to obtain good agreement with the present experimental results. In general, good agreement was obtained between the model and experiments and consistent trends were observed and these are discussed.

Keywords:

rapid compression machine, shock tube, ignition, propylbenzene, ignition delay times, butylbenzene

---

1. Introduction

Heightened awareness of dwindling fuel supplies and of pollutant emissions have resulted in the need to understand the chemistry behind the oxidation of modern transportation fuels. Unfortunately, due to the complex nature of these fuels, they being comprised of hundreds of different individual components, it is difficult to do so. For this reason, the combustion community studies separate fuel components to understand the oxidation of different chemical classes (alkane, alkene, cycloalkane, aromatic, etc.) in a gasoline or diesel fuel. Then they are combined into surrogate fuels that are designed to mimic the combustion of these more complex fuels.

A summary of work carried out on alkylbenzene fuels has been reported previously in our previous study [9] and only a brief summary of the *n*-propylbenzene work is given here.

Burgoyne [1] reported on the products of combustion of a range of n-alkylbenzenes reacting in silica vessels. Results showed that chain mechanisms are heavily involved in the combustion of hydrocarbons but that the chain characteristics of benzene differed significantly when compared to the higher alkylbenzenes [1]. In the second of this series, the ignition of n-alkylbenzenes (including n-propylbenzene) was studied at relatively low temperature (400^{o}C). It was found that thermal characteristics are important for methylbenzenes, but branching reactions play a pivotal role in the ignition of benzene and its mono-alkyl derivatives higher than methyl.

Part three of the series [3] investigated ignition and cool-flame characteristics of a number of alkyl aromatic compounds and found a cool flame ignition was observed near the pressure minimum for *n*-propylbenzene on a temperature-pressure map of cool-flame behavior. The ignition temperature for *n*-propylbenzene was found to be 418^{o}C and an ignition delay time was also reported. In the final part of the series, the slow combustion of benzene and mono-alkyl derivatives was studied. It was found that the oxidation of propylbenzene consists of

two co-existent chain reactions; one was found to predominate below 300°C and the other above 400°C, while in the intervening range of temperature the two mechanisms proceeded at approximately the same rate. The low-temperature reaction on intensification, gives rise to cool flames, while from the high-temperature mechanism a chain-thermal ignition results. At temperatures of 300–400°C the prominence of the process of cool-flame initiation was thought to be the partial cause of the observed increase in the order of reaction, and it was suggested that the negative temperature coefficient was due to the mutual interaction of the co-existent chain reactions [4].

Litzinger et al. [5] used a flow reactor to study the oxidation of *n*-propylbenzene near 1060 K at atmospheric pressure and deduced the reactions involved in removing the *n*-propyl group. Three major routes were found: (i) abstraction of a hydrogen from the propyl group followed by decomposition of the radical and oxidative reactions, (ii) displacement of the propyl group by a radical species, and (iii) direct cleavage of the side-chain followed by the oxidation of the benzyl radical. The reaction sequences beginning with the abstraction of primary and benzylic hydrogen atoms from the propyl group show a strong analogy to results for the oxidation of propane. However, the products predicted based on the analogy to propane for the abstraction of secondary hydrogen atoms from the propyl group were not detected in significant quantities. The absence of expected products led to the recognition that a rapid isomerization of the phenyl propyl radical occurs from the beta to the alpha position on the propyl chain prior to the decomposition of the radical.

Roubaud et al. [6] carried out rapid compression machine experiments on eleven different alkylbenzenes (including *n*-propylbenzene) in the lower temperature region (600–900 K), at compressed pressures of up to 25 bar for stoichiometric mixtures in air. Dagaut et al. [7] carried out experiments in a jet-stirred reactor (JSR) at atmospheric pressure over a temperature range of 900–1250 K at a range of equivalence ratios between 0.5 and 1.5. A

recent study by Gudiyella and Brezinsky [8] produced high-pressure single-pulse shock tube speciation data obtained at shock pressures of 25 and 50 atm, at temperatures between 838–1669 K and equivalence ratios between 0.5–1.9.

Finally, at NUI Galway ignition delay times were measured for mixtures of *n*-propylbenzene in air at equivalence ratios of 0.29, 0.48, 0.96 and 1.92 and at reflected shock pressures of 1, 10 and 30 atm in a heated high-pressure shock tube over a wide temperature range (1000–1600 K) [9]. The effects of reflected shock pressure and of equivalence ratio on ignition delay time were determined and common trends highlighted. These data were also compared with those measured for *n*-butylbenzene and it was found that *n*-propylbenzene was always slower to ignite.

In this study, we have extended our previous work to lower temperatures and higher pressures. We have investigated the low-temperature chemistry (650–1000 K) range for *n*-propylbenzene oxidation at equivalence ratios (ϕ) of 0.29, 0.48, 0.96, and 1.92, and at pressures of 10 and 30 atm. In particular, we provide ignition delay time measurements for *n*-propylbenzene measured in our rapid compression machine (RCM) and compare these times to those obtained previously in our high-pressure shock tube (HPST) and to those from a previously published chemical kinetic mechanism. Additionally, 50 atm data was obtained in both our RCM and in our HPST, for all temperatures and equivalence ratios listed above.

The experimental data presented here for *n*-propylbenzene are also compared to those obtained for *n*-butylbenzene oxidation under similar conditions in a complementary study submitted for publication [10]. These data have been obtained over the same temperature and pressure range and at similar fuel/air equivalence ratios to ensure its viability as a comparison.

2. Experimental

2.1. Rapid Compression Machine

The RCM used here is a clone of the original NUI Galway RCM which is characteristically different to most other RCMs in that it has a twin-opposed piston configuration as described previously [11], resulting in a fast compression time of approximately 16 ms. Additionally, creviced piston heads are used to improve the post compression temperature distribution in the combustion chamber [12]. The design for these creviced piston heads was originally devised at MIT [13, 14], who found that the temperature field obtained using creviced pistons is almost homogeneous compared to that obtained using flat piston heads which is predicted to lead to far greater gas in-homogeneities in the post-compressed combustion chamber. A computational fluid dynamics (CFD) study carried out at NUI Galway [15] supports this view.

In our RCM it is possible to reach different compressed gas temperatures by (i) varying the diluent gas used, typically we use CO_2, N_2 or Ar, (ii) varying the compression ratio, in our case by using different sized piston heads and (iii) using different initial temperatures. We used two different sized piston heads in this study, one with a longer body such that we achieve a compression ratio of approximately 13:1 and another with a smaller body where we achieve an approximate compression ratio of 9.5:1. The 'effective compression ratio' is lowest in argon and highest in carbon dioxide as the diluent gas, due to their relative ratio of specific heats. Using pure CO_2 as the diluent allowed us to measure ignition times at the lowest temperatures, while the use of Ar allows higher temperatures to be studied due to its higher ratio of specific heat, while pure N_2 lies in between these two.

The reaction chamber is wrapped in double-stranded heating tape (Flexelec, 1250 W) which is insulated, and allows the variation of the initial temperature to a maximum of 140 K. By changing (i) the diluent gas composition, (ii) the piston heads and (iii) using the heating

system it was possible to study a compressed gas temperature range of 600–1000 K. However, if the ignition delay times are limited to those below about 100 ms due to excessive heat losses, the minimum temperature achievable for *n*-propylbenzene is approximately 750 K.

The heating system is also installed on the manifold and mixing tanks, to ensure that *n*-propylbenzene, which has a saturation vapour pressure of 0.5 kPa at 25^{o}C [16], does and did not condense in the experiments. The manifold is heated by first attaching "type K" thermocouples at various locations along the manifold. Flexelec heating tapes are wrapped around the manifold and these were covered with Zetex 1000 insulation tape. The thermocouples were connected to both the heating tapes via a Cal 9900 thermostat and a Pico TC-08 USB thermocouple data logger (which in turn was connected to a PC). The temperatures in the manifold were monitored to keep the reactant mixtures above the saturation temperature of *n*-propylbenzene at the reactant pressure at all times.

Pressure-time profiles are measured using a pressure transducer (Kistler 603B) and transferred via an amplifier (Kistler 5018) to an oscilloscope (Picoscope 4424) and ultimately recorded digitally on computer using the Picolog PC software. The non-linearity of the pressure transducer is less than ±1% of the full scale output. The ignition delay time, defined as the time from the peak pressure near the end of compression to the maximum rate of pressure rise during ignition, is measured using two vertical cursors on the oscilloscope. In general, it was found that the ignition delay times were reproducible to within 15% of one other at each compressed temperature. The compressed gas pressure was measured using two horizontal cursors.

The time for compression is fast, ≈16 ms, with most of the rapid rise in pressure and temperature taking place in the last 2–3 ms of compression; therefore heat losses during compression are small but do exist. For a period following compression, the gases experience

a high degree of heat loss owing to the swirl experienced and the high temperature of the gas within the chamber. Heat losses continue from the core gas during the constant volume period. For this reason, non-reactive pressure traces are taken to account for these heat losses in simulations of the RCM ignition experiments. These non-reactive pressure traces replace the oxygen content with inert nitrogen. A typical pressure-time trace obtained on the rapid compression machine is shown in Fig. 1. The reactive pressure trace is represented by the solid line while the non-reactive trace is depicted by the red dashed line.

The compressed gas temperature, T_C, was calculated using the initial temperature, *Ti*, pressure, p_i and reactant composition and the experimentally measured compressed gas pressure, p_c, defined as the maximum pressure immediately after compression, and employing the adiabatic compression/expansion routine in Gaseq [17], which uses the temperature dependence of the ratio of specific heats, γ, according to the equation:

$$\ln\left(\frac{p_C}{p_i}\right) = \int_{T_i}^{T_c} \frac{\gamma}{\gamma - 1}\frac{dT}{T}$$

while assuming frozen chemistry during compression. The compressed gas temperature is then plotted against the measured ignition delay time to obtain overall reactivity profiles of *n*-propylbenzene.

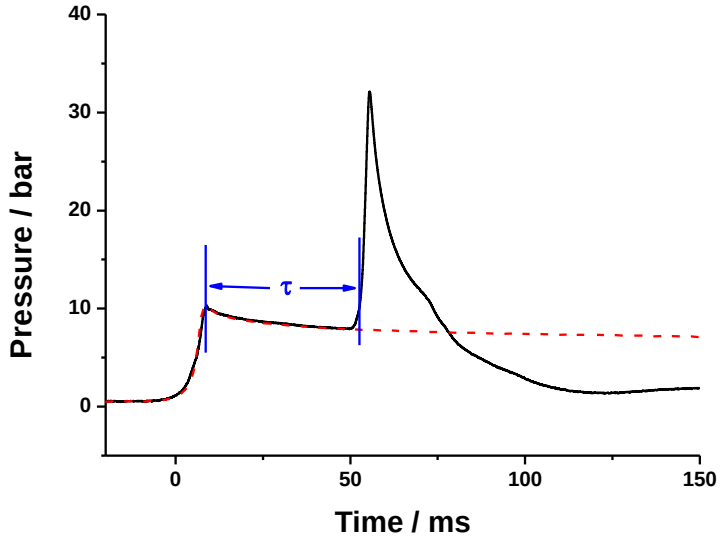

Figure 1: Typical pressure trace obtained from the NUIG rapid compression machine; ϕ = 2.0, p_C = 10 atm, T_C = 842 K, ignition delay time = 41.7 ms. Solid line represents reactive mixture, while the dashed line represents the non-reactive mixture.

2.2. High-Pressure Shock Tube

Ignition delay times were measured at high temperature using our new HPST facility. Our previous shock tube [9] was unable to withstand the 50 bar reflected shock pressures presented here and thus a new HPST facility was designed to withstand reflected shock pressures of approximately 100 bar. Ignition delay times at 50 bar were obtained in the new shock tube. Preliminary experiments at 10 and 30 bar were conducted and the new shock tube reproduced identical results compared to those obtained in the previous shock tube.

The dimensions of the new shock tube are the same as those for the previous shock tube (9.0 m in length; 63.5 mm in internal diameter). A double-diaphragm section divides the shock tube into a 3 m long driver section and a 5.7 m driven section. Aluminium plates were used as the diaphragm, where diaphragms of various thicknesses are chosen depending on the desired final shock pressure and vary in thickness from 0.8–2.0 mm. A helium (99.99% pure; BOC) and nitrogen (99.99% pure; BOC) mixture were used as the driver gas, where the mixing ratio was chosen depending on the desired final shock pressure and test duration and

varied from approximately 75:25 to 100:0 (He:N_2). Six pressure transducers on the sidewall (PCB; 113A24), located at known distances from the endplate, and one at the endwall (Kistler; 603B) were used to measure the velocity of the incident shock wave, which was used to calculate temperature of mixtures behind the reflected shock wave using Gaseq [17]. Pressures behind the reflective shock wave were measured using the pressure transducer located at the endwall. Pressure traces were obtained using two digital oscilloscopes (TiePie Handyscope HS4).

The ignition delay time was defined as the interval between the rise in pressure due to the arrival of the incident shock wave at the endwall and the maximum rate of rise of the pressure signal. Some example pressure traces are shown in Figure 2; in this figure two pressure traces achieved at ϕ = 1.92 and 50 atm are illustrated. A facility effect was observed in the experiments which resulted in a maximum of 3% / ms increase in pressure before ignition for all experiments. A significant pressure rise before the autoignition event, i.e. an indication of inhomogeneous pre-ignition, was not observed in the present experiments.

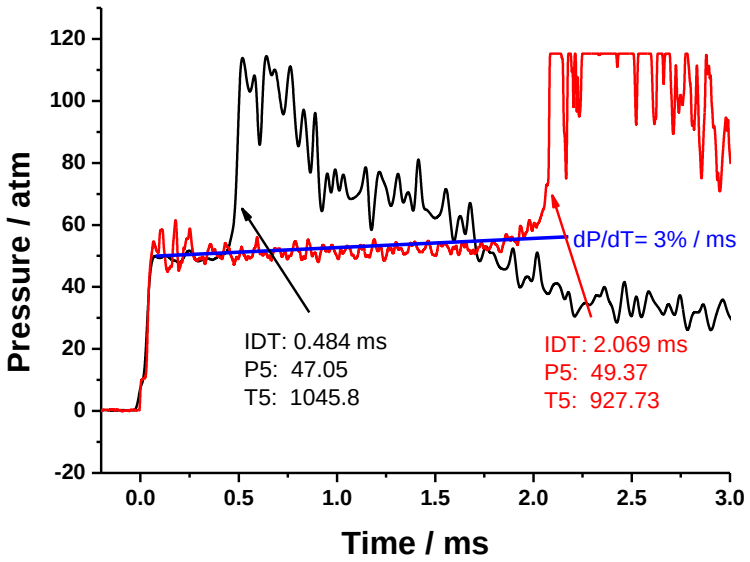

Figure 2: Typical pressure traces obtained from the NUIG high pressure shock tube; Red trace; ϕ = 2.0, p_5 = 49.4 atm, T_C = 927 K, ignition delay time = 2.07 ms, Black trace; ϕ = 2.0, p_5 = 47.1 atm, T_5 = 1045 K, ignition delay time = 0.484 ms.

A heating system was designed and installed on the driven section and manifold of the shock tube and the shock tube was heated to a maximum of 130ºC to ensure that no condensation *of n*-propylbenzene, which has a saturation vapor pressure of 0.5 kPa at 25^{o}C [16], occurred.

2.3. Mixture Preparation

The gas mixtures and the initial conditions studied are documented in Table 1.

Table 1: Molar composition of *n*-propylbenzene mixtures studied.

ϕ	% fuel	% O_2	% Diluent
0.29	0.50	20.89	78.61
0.48	0.83	20.83	78.34
0.96	1.65	20.65	77.70
1.92	3.25	20.32	76.43

The gases used, nitrogen (CP Grade) 99.99%, argon (Research Grade) 99.99%, oxygen (Medical Grade) 99.5%, were supplied by BOC Ireland and were used without further purification. *n*-Propylbenzene was obtained from Tokyo Chemicals Ltd at 99% purity (GC grade) and used without further purification.

As *n*-propylbenzene is a liquid fuel at room temperature mixtures were prepared by a direct injection method. In this method the fuel was injected via an injection port on the top of the heated mixing tanks using a gas-tight syringe (SGE Analytical Science, 5ml volume, 008760). The determined amount of fuel was added based on its appropriate weight and the partial pressure of fuel was measured using an MKS pressure transducer and digital readout followed by the addition of oxygen and nitrogen to the desired partial pressures.

All mixtures were left for at least one hour before use in both the RCM and in the HPST to ensure homogeneous charge composition. Mixture compositions were verified by in-situ testing using an infra-red laser system similar to that of Mével et al [18] who studied gas phase absorption cross sections at 3.39 μm to determine the concentration of twenty-one liquid hydrocarbons in the temperature range 303–413 K using an infrared He–Ne laser, Fig.

3. Estimated uncertainty limits of the measurements are ± 1% in reflected shock temperature, T_5, ± 15% in ignition delay time, τ, and ± 2 % in mixture composition.

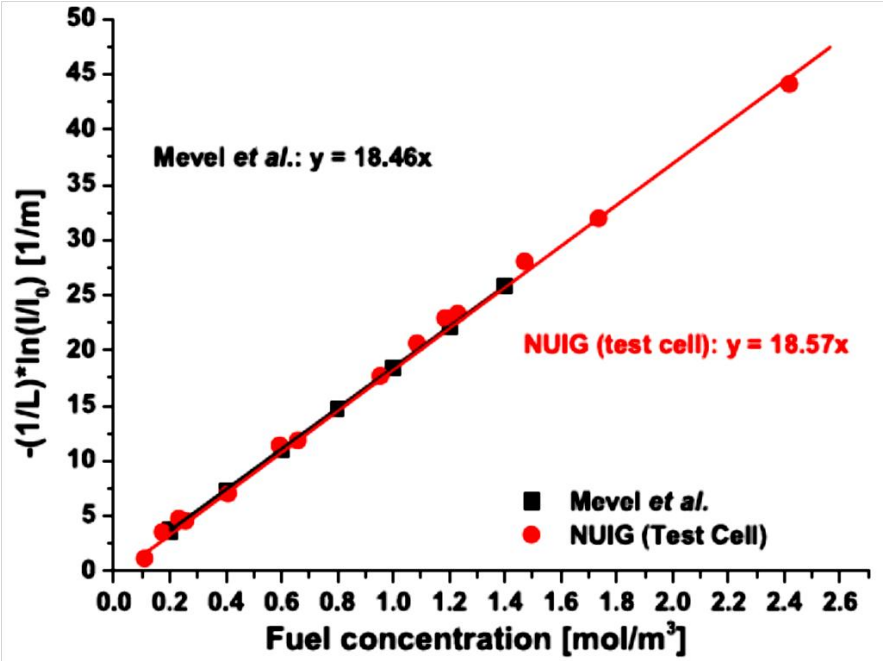

Figure 3: Comparison of the evolution of $-(1/L).\ln(I/I_0)$ as a function of the *n*-propylbenzene concentration calculated in this study and by Mével et al. [18].

3. Results

3.1. Chemical Kinetic Model

The chemical kinetic model discussed in this paper has been initially derived merging the recently published C_0–C_4 kinetic mechanism developed at Galway (AramcoMech 1.3) [19] with the toluene mechanism by Metcalfe et al. [20] and with the alkyl-aromatic sub-mechanism published previously by Darcy et al. [21]. Improvements to this initial merged mechanism have been made and are described below.

The original mechanism by Metcalfe et al. [20] has been extended to include more detailed cyclopentadiene chemistry, including the addition of the cyclopentadienyl ($\dot{C}_5H_5$) radical on cyclopentadiene (C_5H_6) and the recombination of $\dot{C}_5H_5$ radicals to form larger aromatic species. The thermal properties for the toluene sub-mechanism were obtained from [20].

Reaction rates for these reactions were derived from the theoretical study on cyclopentadienyl radical reactions performed by Cavallotti et al. [22]. In order to achieve a satisfactory agreement with the flow reactor data presented in the experimental study by Butler and Glassman [23], the recommended reaction rates proposed by Cavallotti was multiplied by a factor 2. A more extensive description of heavier aromatic species, such as indene and naphthalene has also been introduced, including the reactions leading to the formation and the subsequent oxidation of naphthalene and indene. The sub-mechanism for these polycyclic aromatic species has been derived from the Narayanaswamy et al. mechanism [24]. These additions improved the agreement between the predictions of the modified mechanism and the cyclopentadiene experimental data available in the literature [23].

The alkyl aromatic mechanism (including ethylbenzene, *n*-propylbenzene and *n*-butylbenzene) is based on the mechanism proposed by Diévart and Dagaut [25]. In our prior work [9], the *n*-propylbenzene portion of the model was updated by revising the reaction rate constants for the hydrogen abstractions on the alkyl chain of the fuel. Because site-specific H-atom abstraction rate constants for n-propylbenzene were not available, rate constants for the secondary benzyl hydrogen atoms were matched to the reaction rate of secondary allyl hydrogen atoms of 1-pentene, and secondary and primary hydrogen abstraction rates to the analogous reaction rates of alkane species. The secondary benzyl radical + $H\dot{O}_2$ reaction leading to the formation of the benzoxy and radicals has been set to $1 \times 10^{13}\,cm^3\,mol^{-1}\,s^{-1}$, as proposed in [20] for the benzyl radical of toluene. Beta-decomposition reactions of the phenyl-propyl radicals were specified in the exothermic direction.

In this work, a low temperature mechanism for *n*-propylbenzene has been developed so that the mechanism can be used to simulate low temperature ignition in an RCM. Reaction rates for the low temperature branching paths active on the alkyl chain of the fuel molecules were derived from the alkene mechanism by Mehl et al. [26], assuming that allylic site in the

olefin chain corresponds to the benzylic one present in the aromatic structures. Internal isomerization rates for *n*-propylbenzene were assumed to match the corresponding rates adopted for 1-pentene.

The addition reactions of the benzyl radical to molecular oxygen, an important step in the low temperature mechanisms of alkylbenzenes in general have been derived fitting in the temperature of interest (600–900 K) the reaction rates that have been theoretically calculated by Murakami et al. [27] for the xylyl + O_2 system. The reaction rate for the concerted elimination of $H\dot{O}_2$ from the alkylperoxy species have been derived from Altarawneh et al. [28], who theoretically studied the low temperature oxidation of ethylbenzene. The proposed value of ($1 \times 10^{11} \times T^{0.76} \times \exp(-27221/\mathrm{RT}) \ s^{-1}$) was reduced by a factor 2, within the uncertainty of the method used in the calculations to improve agreement with the RCM experiments. Reverse rates for these reactions are calculated from the thermodynamic properties.

The thermodynamic properties for the low temperature species involved in the *n*-propylbenzene mechanism was estimated using the THERM program developed by Ritter and Bozzelli, implementing Benson's group additivity method [29, 30]. These estimations corrected significant errors in the thermodynamic parameters for the low temperature *n*-butylbenzene species compared to the previous model. Also, critical $\dot{R}–O_2$ bond energies were updated with the THERM estimates.

The thermodynamic properties for the low temperature species involved in the *n*-propylbenzene mechanism was estimated using the THERM program developed by Ritter and Bozzelli, implementing Benson's group additivity method [29, 30]. These new estimations corrected significant errors in the thermodynamic parameters for the low temperature *n*-butylbenzene species compared to the previous model. Also, critical $\dot{R}–O_2$ bond energies were updated with the new THERM estimates.

The group values used to evaluate the thermal properties of the propylbenzene low temperature species were mostly the ones distributed with the early 90s version of THERM. Although the authors are in the process of updating some important entries in the group and bond's databases using more recent group values from literature or from personal communications with Bozzelli et al., in this specific case all the groups needed were available in the original version of the database. It is noteworthy that in the "standard" database we used, CD carbons are typically assumed to be similar to CB carbons.

For the alpha radical (4-phenylbut-4-yl radical)–O_2 (secondary benzylic), the new value resulting from the updated THERM calculations is now 23.7 kcal mol^{-1}, a value close to the 24.6 kcal mol^{-1} calculated by [28]. This bond energy is significantly higher than the one calculated for a primary benzylic $\dot{R}–O_2$ bond (19.7 kcal mol^{-1}) based on the thermodynamic properties we are using for benzyl and $\dot{R}O_2$ radicals [20]. It is worth stressing how these values are significantly lower than the bond strength calculated for non-resonantly stabilized secondary alkyl radicals (38 kcal mol^{-1}). The correct evaluation of the relative bond energies in the $\dot{R}–O_2$ for alkyl aromatic systems (secondary benzylic $\dot{R}–O_2$ compared to the primary benzylic, compared to the secondary alkyl) is an important factor in reproducing the experimental behavior observed in the NTC region and in showing the significance of the addition of the alpha radical (4-phenylbut-4-yl radical) to molecular oxygen and subsequent low temperature branching reactions. This important point will explained in more depth in the discussion section. The resulting mechanism includes about 960 species and 4330 and is included along with thermodynamic properties in the Supplemental Material.

RCM experiments were simulated using CHEMKIN-Pro [31]. For the ignition calculations in an RCM, the calculations use volume profiles generated from the non-reactive pressure traces. The volume history is used to simulate the compression stroke and the heat losses that occur during the experiments. The calculations are performed using a zero-dimensional

model that assumed and assumes an ‘adiabatic core’, an approach described by Mittal et al. [32]. All non-reactive pressure traces are available as Supplemental Material.

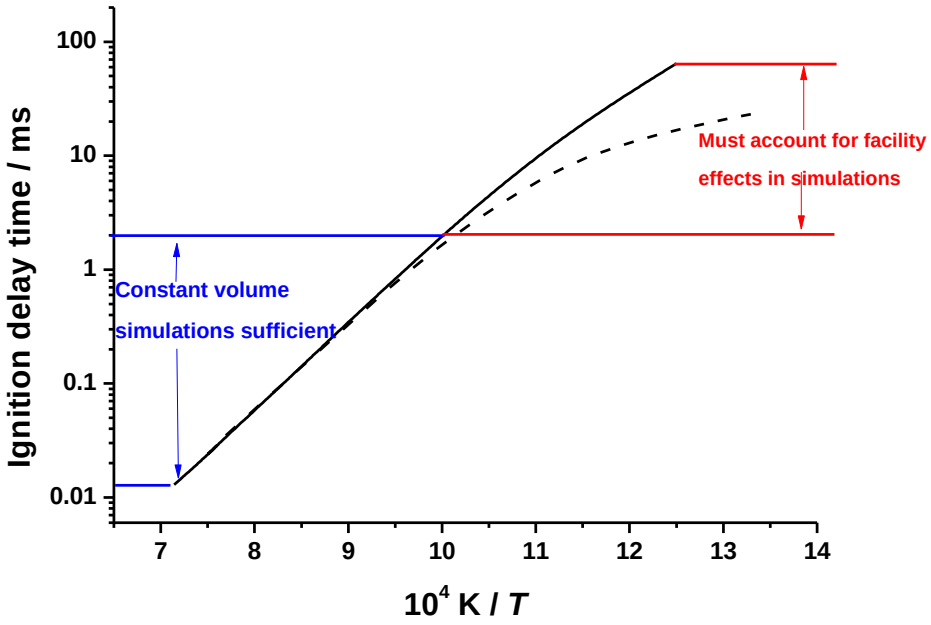

Figure 4: Simulations carried out at ϕ = 0.48, 50 atm. Solid line represents simulations assuming adiabatic, constant volume conditions while dashed line represents simulations accounting for a 3% pressure increase per millisecond gradient over the entire temperature range.

HPST simulations were also carried out using CHEMKIN-Pro, with reflected shock temperature and pressure used as initial conditions. Calculations were performed with the constant volume approximation and with facility effects to determine the regimes when facility effects are significant. The 3% / ms increase in pressure witnessed in the experiments was simulated in a similar manner to the rapid compression machine simulations where a volume profile was generated to account for this pressure increase. We observed very little variation between predicted ignition delay times using (i) adiabatic, constant volume simulations, and (ii) including the 3% / ms pressure rise due to the relatively short ($\leq$ 2 ms) measurement times of these experiments. It is important to account for these facility effects

for longer ignition times, but as the experimental data obtained in this study are within this range adiabatic simulations suffice, Fig 4.

3.2. n-Propylbenzene oxidation results

Figures 5 and 6 compare simulations with the experimental data. Error bars of ± 15% in ignition delay times in the experimental data are given to account for experimental uncertainties. Complete tables of our experimental data can be found in the Supplemental Material. In these figures, solid symbols represent shock tube experiments while open symbols represent RCM experiments. Solid lines are used on the graphs to show constant-volume, adiabatic simulations while the dashed lines illustrate the simulations using volume histories from the RCM to account for the facility effects of the RCM. There is reasonable agreement observed between model and experiments throughout the study which indicates that the updated and extended chemical kinetic mechanism captures the general trend in reactivity of these fuel mixtures. In the next sections, the effects of pressure and equivalence ratio on the ignition delay times are discussed in turn.

3.2.1. Influence of compressed pressure on ignition delay time

The effect of pressure on ignition delay times was studied at four different fuel / air equivalence ratios (0.29, 0.48, 0.96 and 1.92), Fig. 5. Ignition delay times of *n*-propylbenzene oxidation versus inverse temperature at an equivalence ratio of 0.29 and at pressures of approximately 1, 10, 30 and 50 atm are shown in Fig. 5(a). At these conditions, fuel reactivity increases with increasing pressure and shorter ignition delay times were measured for higher pressures. The same trends are observed for fuel/air mixtures at equivalence ratios of 0.48, 0.96 and 1.92 at the same reflected shock pressures, Figs. 5(b) – 5(d). This indicates a consistent trend of increasing reactivity of *n*-propylbenzene with increasing pressure throughout this study. These results are typical of the effect of pressure on ignition delay time for other hydrocarbons [33].

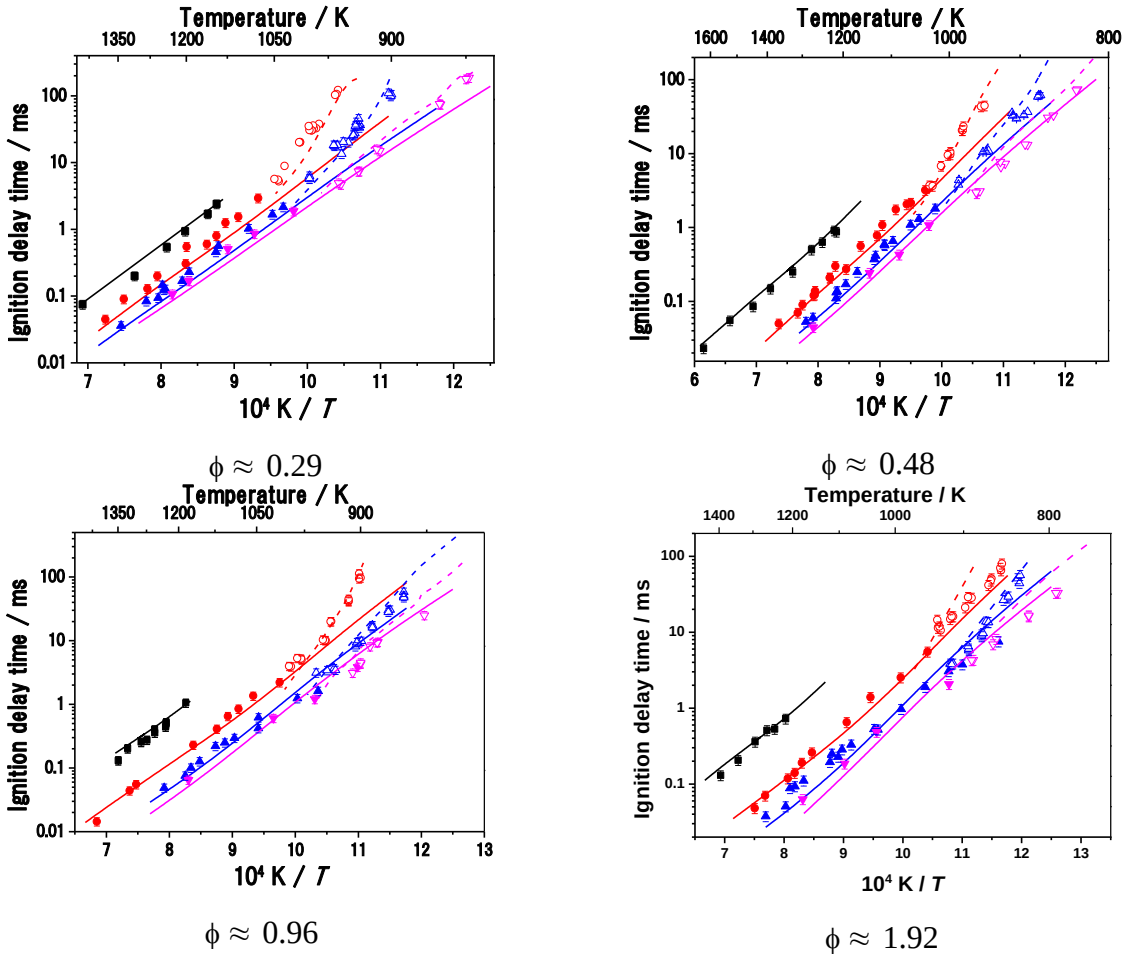

Figure 5: Effect of varying reflected shock pressure on *n*-propylbenzene reactivity; ■– 1 atm, ●– 10 atm, ▲– 30 atm. ▼– 50 atm. Solid symbols: Shock tube, Open symbols: RCM. Simulation; – – – RCM simulations including facility effects, — adiabatic, constant volume simulations.

The chemical kinetic model is able to simulate the effect of pressure reasonably well over the temperature and pressure range. The largest deviations (about a factor of two) were in the low temperature region covered by the RCM experiments and at the highest pressures. Adiabatic simulations show a slight curvature in the ignition delay times for the rich and high pressure cases. This is caused by the low temperature low temperature degenerate branching pathways we introduced in the mechanism which enhance the reactivity of the fuel in the low

temperature region. No negative temperature coefficient behavior is experimentally observed for *n*-propylbenzene. This is consistent with the observations of Roubaud et al. [6] in their study of the oxidation of a wide variety of alkyl-aromatic compounds.

3.2.2. Influence of equivalence ratio on ignition delay time

The effect of equivalence ratio on ignition delay times was determined for four fuel/air mixture compositions at 10, 30 and 50 atm, Fig. 6. Experiments at 1 atm were omitted from Fig. 6 because they were only possible using the shock tube and not using the RCM. The shock tube results can be found in a previous publication [9]. The effect of equivalence ratio at pressures of 10 atm at the four equivalence ratios studied (0.29, 0.48, 0.96 and 1.92) is shown in Fig. 6(a). At intermediate temperatures (about 800-1200 K, depending on pressure) fuel-rich mixtures ignite faster than fuel-lean ones. This behavior at intermediate temperatures is attributed to the chain branching sequence RH + $H\dot{O}_2$ = $\dot{R}$ + H_2O_2 followed by H_2O_2 (+M) = $\dot{O}H$ + $\dot{O}H$ (+M), where RH is the fuel components. In the present experiments, the equivalence ratio is increased by increasing the fuel concentration ([RH]) which enhances the rate of this branching sequence that produces two reactive $\dot{O}H$ radicals. Traditional low temperature behavior including an NTC region showing negative slope on an Arrhenius plot was not observed for pure *n*-propylbenzene experiments. The experimental behavior at low temperature is well captured by the kinetic model.

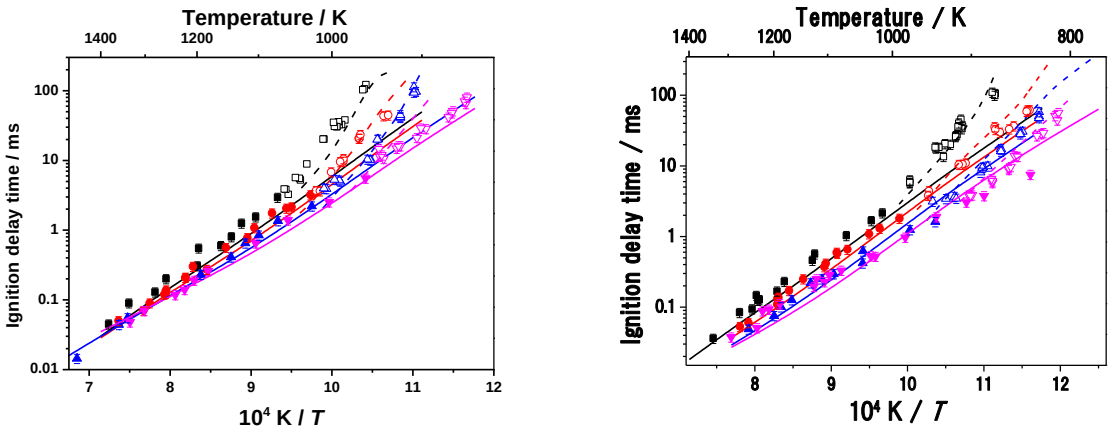

(a) 10 atm (b) 30 atm

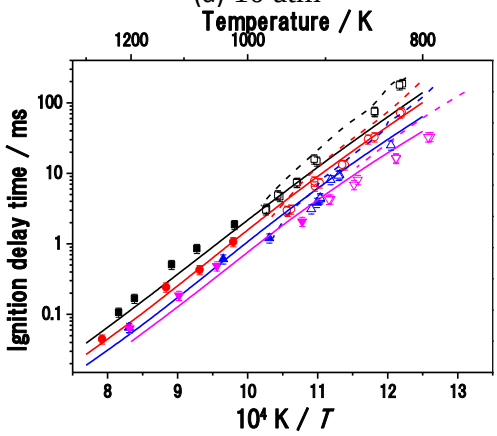

(c) 50 atm

Figure 6: Effect of varying equivalence ratio (ϕ) on *n*-propylbenzene reactivity; ■– ϕ = 0.29, ●– ϕ = 0.48, ▲– ϕ = 0.96, ▼– ϕ = 1.92. Solid symbols: Shock tube, Open symbols: RCM. Simulation; – – – RCM simulations including facility effects, — Adiabatic, constant volume simulations.

At high temperatures (about 1050 to 1400 K), the difference between the mixtures is much smaller relative to that at the low and intermediate temperatures. However, if one looks closely enough at the relative slopes of the data it can be concluded that there is a convergence of the all data sets at the highest temperatures studied for 10 atm experiments, Fig 6(a). In the case of the 30 and 50 atm experiments and judging by the relative slopes of each data set, this convergence of data will occur at a higher temperature than is achievable in this study due to the short ignition delay times observed in the experiments. The convergence is due to the increasing importance of the chain-branching reaction $\dot{H} + O_2 = \ddot{O} + \dot{O}H$ at higher temperatures. At higher temperatures, the reaction of the fuel with H atoms ($RH + \dot{H} = \dot{R} + H_2$) competes with the branching reaction for H-atoms. When the equivalence ratio is increased, the fuel concentration [RH] is increased. At a higher [RH], RH + H competes more effectively for H atoms and causes ignition delay times to be longer than they would be been otherwise. This effect of equivalence ratio is opposite of that caused by the $RH + H\dot{O}_2 = \dot{R} + H_2O_2$ reaction discussed above. These two effects cancel out and lead to a convergence of

the experimental data and the modeling results at the temperature is increased at higher temperatures.

4. Discussion

As the simulations achieved using the chemical kinetic mechanism agree with the experimental data it is now possible to use this mechanism to explore the important chemistry determining the reactivity of this fuel.

A flux analysis was carried out at $\phi = 0.96$ and 10 atm for a series of temperatures (750, 1000 and 1400 K) and 15% fuel consumed, these being most representative for the experimental conditions studied. This was performed to investigate the important reactions occurring at varying temperatures for *n*-propylbenzene oxidation.

This flux analysis (Fig. 7) covers the most common reactions occurring at various temperature regimes, the numbers in black font represent the percent fuel flux at 1500 K, while red numbers represent the flux at 1000 K and blue numbers represent the flux at 750 K. Included in the flux are the names of as denoted in the chemical kinetic mechanism. These were included to assist in the discussion below and to allow searching for specific reactions within the mechanism that is included as Supplementary data.

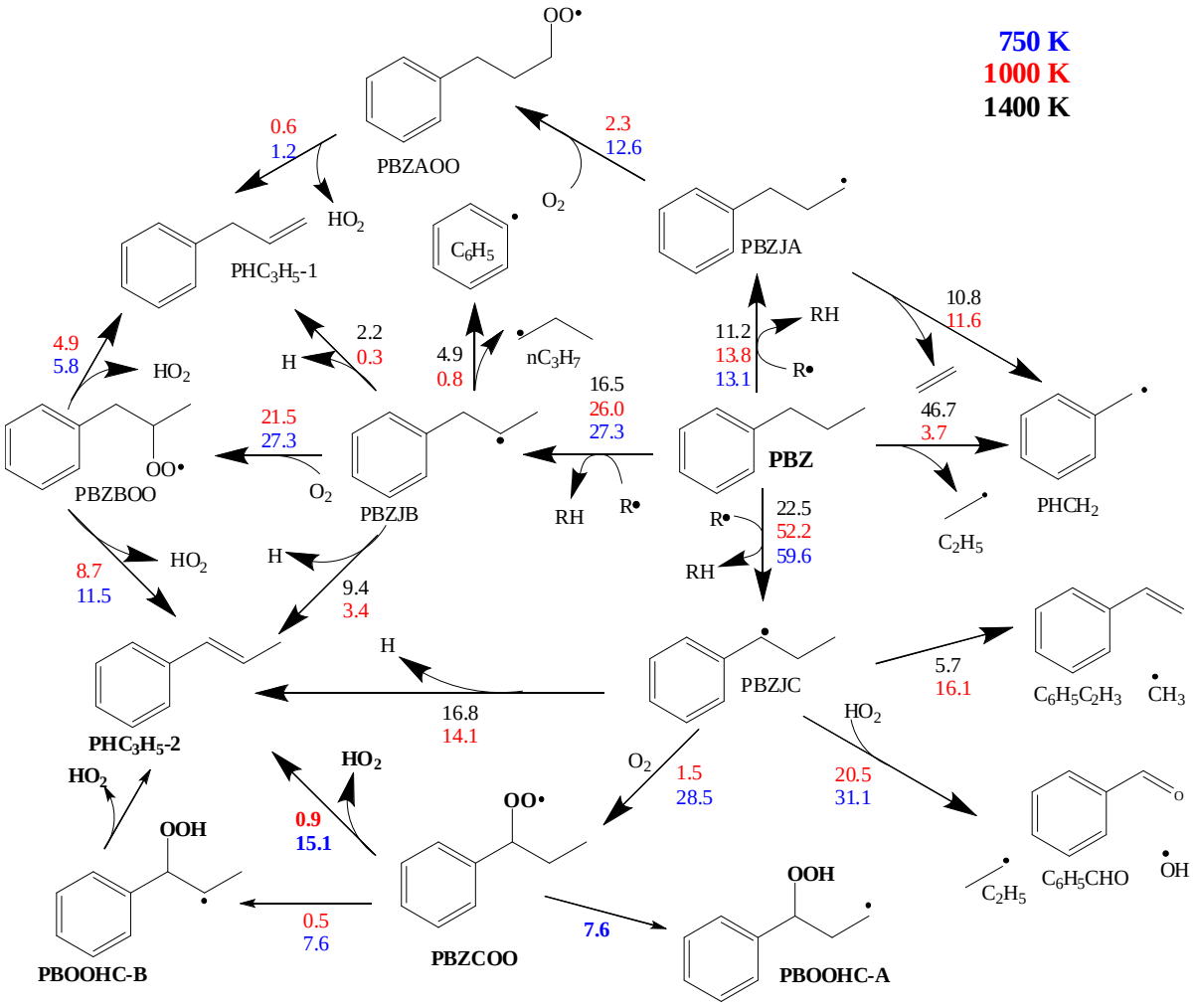

Figure 7: Flux analysis carried out for *n*-propylbenzene (PBZ) oxidation at ϕ = 0.96, 10 atm and 15% fuel conversion. Numbers represent the percent of fuel flux that goes through a particular species. Black numbers represent flux at 1400 K, Red numbers represent flux at 1000 K and Blue numbers represent flux at 750 K. R is the sum of $\dot{H}$, $\dot{O}$, $\dot{O}H$, $H\dot{O}_2$ and $\dot{C}H_3$.

At an intermediate temperature of 1000 K (numbers in red font), the main consumption pathways for *n*-propylbenzene are abstraction reactions on the alkyl chain, mainly by $\dot{O}H$ radicals. A strong selectivity on the 2-phenyl-2-propyl (allylic) site is observed, accounting for 52.2% on the total abstraction rate. The primary site (designated by A in the species PBZJA), is the least targeted by abstraction and, due to the weakness of the allylic C–C bond in the PBZJA formed, it rapidly decomposes to benzyl radicals and ethylene. Additionally the radical is consumed via radical addition to molecular oxygen followed by a concerted elimination reaction forming 1-propenylbenzene and $H\dot{O}_2$ radical. This occurs to a much

lesser extent (2.3%) at 1000 K compared to the β-scission reaction which forms ethylene and benzyl radicals (11.6%).

When abstraction occurs on the secondary site (forming PBZJB), the radical is mainly consumed via addition to molecular oxygen followed by the concerted elimination pathway, showing a selectivity of 2:1 towards the formation of 2-propenylbenzene (PHC_3H_5-2) versus 1-propenylbenzene (PHC_3H_5-1) and $H\dot{O}_2$ radicals. The value of the selectivity to 2-propenylbenzene was specified using a recently calculated rate constant for the corresponding concerted elimination rate constant from Altarawneh et al. [28]. Additionally the PBZJB radical can decompose directly to form both the 1-propenylbenzene (0.3%) and 2-propenylbenzene radicals (3.4%) together with hydrogen atoms, but this is much less important compared to the radical addition / concerted elimination route which generates 8.7% 2-propenylbenzene and 4.9% 1-propenylbenzene respectively.

The predominant 2-phenyl-2-propyl radicals (labelled as PBZJC), are mainly consumed (20.5%) via reaction with $H\dot{O}_2$ radicals leading to the formation of benzaldehyde and hydroxyl and ethyl radicals. Because of the intrinsic stability of 2-phenyl-2-propyl radicals, their addition to molecular oxygen and subsequent concerted elimination leading to $H\dot{O}_2$ radical formation is less favored compared to a secondary site, and only 1.5% of the initial PBZJC formed follows this pathway. Other important pathways involving the 2-phenyl-2-propyl radical are the two decomposition reactions leading to methyl radical and styrene (16.1%) and to 2-propenylbenzene and a hydrogen atom (14.1%). The rate constants for these decomposition channels were specified in the reverse, exothermic direction as addition reactions of a radical on a double bond. The rate of addition of $\dot{C}H_3$ on styrene was based on the addition of $\dot{C}H_3$ on 1,3-butadiene because both reactions form a resonantly stabilized radical. Similarly, the addition of $\dot{H}$ on a double bond producing the same secondary benzyl radical (PBZJC), was compared to the 1,3-C_6H_{10} + $\dot{H}$ reaction, which results in a secondary

allyl radical (1,3-C_6H_{11}). The resulting decomposition rates, computed from reverse rates using thermodynamic properties, preferred the formation of $\dot{C}H_3$ radicals at low temperature and $\dot{H}$ formation at high temperature (above 1100 K) due to a higher frequency factor and activation energy associated with the $\dot{H}$ atom formation pathway.

At 750 K, the addition of PBZJC to O_2 to form PBZCO$\dot{O}$ is significant (28%) compared to 1.5% at 1000 K. It undergoes an isomerization to PBOOHC-A which is the most sensitive reaction at 750 K identified later in the sensitivity analysis section. These two steps correspond to traditional low temperature chemistry of addition of O_2 to a fuel radical to form "R$\dot{O}_2$" and isomerization to "QOOH" [34]. The PBOOHC-A species undergoes a beta-scission reaction (not shown) to C_6H_5CHO, C_2H_4 and $\dot{O}H$. Because of the production of a reactive $\dot{O}H$ radical, this reaction is also identified later in the sensitivity analysis. An alternative to the beta-decomposition would be the formation of a four-membered ring cyclic ether with the elimination of an $\dot{O}H$ radical. Although both the reaction pathways were included in the mechanism, the decomposition of a PBOOHC-A radical resulted to be dominant due to the presence of a weak allylic C–C bond on the chain of the PBOOHC-A radical. Normally, the formation of a cyclic-ether is energetically favored in alkane like structures; in the case of propylbenzene, the higher frequency factor associated with the beta decomposition coupled with the energetic effects of the weaker C–C bond leads preferably to the C–C bond scission and to the formation of benzaldehyde.

The other fate of the PBZCO$\dot{O}$ radical is to eliminate H$\dot{O}_2$ and form 2-propenylbenzene (15.1%) or to isomerize to PBOOHC-B (7.6%). This later isomerization involving a 5-membered ring is not important for alkanes [35] but is important here due to the weakness of the C–H bond at a secondary allylic site (88.6 kcal mol^{-1}) compared to that at a secondary site

in an alkane (98.5 kcal mol^{-1}) [29]. This effect of this weakness is reflected in the rate constant from Altarawneh et al. [28].

At high temperature (1400 K), unimolecular decomposition of the fuel dominates and abstraction reactions (now mostly involving hydrogen atoms) are less selective, attacking with a similar rate at all of the three sites on the alkyl chain (650 K: PBZJA / PBZJB / PBZJC 13.1 / 27.3 / 59.6% 1000 K: PBZJA / PBZJB / PBZJC 13.8 / 26.0 / 52.2%, 1400 K: PBZJA / PBZJB / PBZJC 11.2 / 16.5 / 22.5%). Abstraction reactions are followed by β-scission reactions leading primarily to ethylene and benzyl radicals, styrene and a methyl radical and 2-propenylbenzene and a hydrogen atom.

4.1. Sensitivity Analyses

Using CHEMKIN-Pro, a brute force sensitivity analysis of different reaction rate constants was computed at the 750 and 1400 K, representing the two extremes of temperatures of this work, at 10 atm and ϕ = 0.96. The analyses were performed by increasing and decreasing both the forward and reverse rate constants by a factor of two, with sensitivities expressed using the formula:

$$S = \frac{\ln(\tau_+/\tau_-)}{\ln(k_+/k_-)} = \frac{\ln(\tau_+/\tau_-)}{\ln(2/0.5)}$$

A positive sensitivity coefficient indicates an inhibiting reaction while a negative sensitivity coefficient relates to a reaction promoting reactivity, Fig. 8. This analysis was carried out for all of the reactions in the mechanisms. Reactions with sensitivity coefficients higher than 0.1 and lower than –0.1 are shown in Fig. 8.

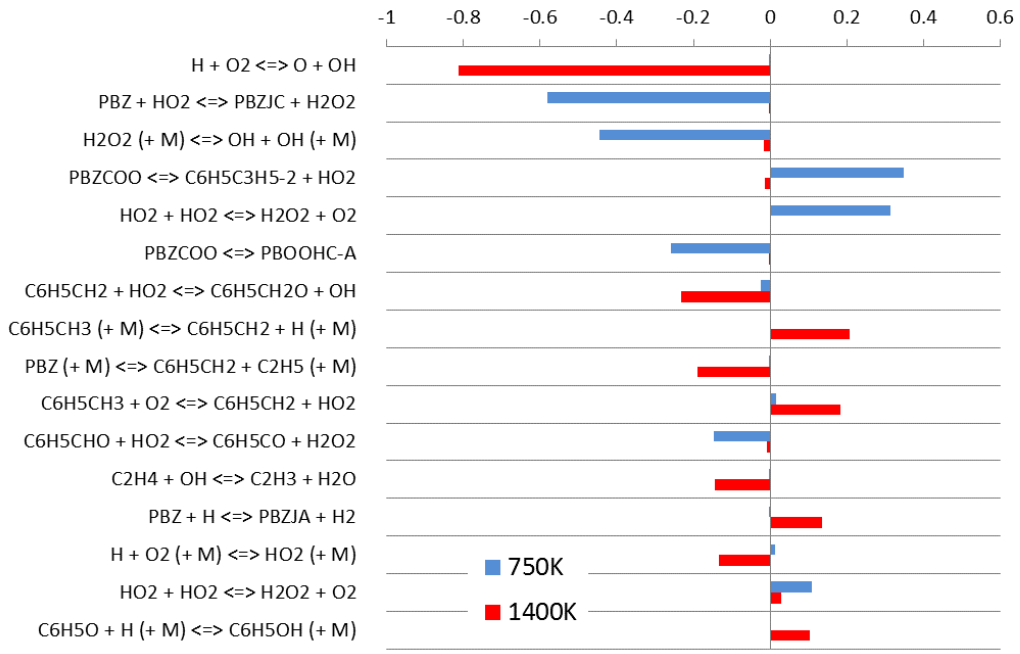

Figure 8: Sensitivity coefficients, *S*, showing the effect of temperature on *n*-propylbenzene ignition delay time, $\phi = 0.96$, $p_5 = 10$ atm.

Two important reactions involved in the low temperature oxidation of propylbenzene that appear in the sensitivity analysis are the $R\dot{O}_2$ isomerization reaction PBZCO$\dot{O}$= PBOOHC-A (discussed earlier in the path analysis results shown in Fig. 7) and the $H\dot{O}_2$ elimination. The isomerization reaction of the $R\dot{O}_2$ radical makes possible the conversion of the resonantly stabilized secondary benzyl radical to benzaldehyde, ethylene and the highly reactive $\dot{O}H$ radical, promoting the reactivity. The competing channel of PBZCO$\dot{O}$radicals at 750 K is the $H\dot{O}_2$ elimination reaction, PBZCO$\dot{O}$= $C_6H_5C_3H_5$ + $H\dot{O}_2$. The $H\dot{O}_2$ radicals produced then react via a radical termination reaction, $H\dot{O}_2$ + $H\dot{O}_2$ = H_2O_2 + O_2. These two reactions strongly inhibit reactivity at 750 K. The most sensitive reaction accelerating ignition at 750 K is the H-atom abstraction reaction with $H\dot{O}_2$ radicals, PBZ + $H\dot{O}_2$ = PBZJC + H_2O_2. The H_2O_2 so produced decomposes to two $\dot{O}H$ radicals, H_2O_2 (+M) = $\dot{O}H$ + $\dot{O}H$ (+M), and this reaction shows the third most sensitive reaction promoting reactivity at 750 K. Low temperature

reactions related to $R\dot{O}_2$ radicals discussed above have a significant impact on ignition delay times. Therefore, the low-temperature oxidation is necessary to accurately predict ignition delay times although *n*-propylbenzene did not show negative temperature coefficient behavior.

At the higher temperatures, the most sensitive step is $\dot{H} + O_2 = \ddot{O} + \dot{O}H$. The third most sensitive reaction is the unimolecular decomposition of *n*-propylbenzene to form benzyl and an ethyl radical which occurs quickly at high temperature due to the weakness of the C–C bond broken (78.4 kcal mol^{-1}). In the flux analysis (Fig. 7), this reaction dominates the consumption of the fuel (46.7% at 1400 K). This reaction promotes reactivity as it leads to the formation of ethyl radicals which decompose to form ethylene and a hydrogen atom. Additionally the benzyl radical reacts with the hydroperoxyl radical to form $C_6H_5CH_2\dot{O}$ radical and an hydroxyl radical which is the second sensitive reaction promoting ignition as it can abstract hydrogen atoms from relatively stable molecules, for example *n*-propylbenzene. The reaction of the fuel with $\dot{H}$ atom at 1400 K are inhibitory, due to their competition with the most sensitive reaction at high temperature, the chain branching reaction $\dot{H} + O_2 = \ddot{O} + \dot{O}H$.

5. Conclusions

A comprehensive study of *n*-propylbenzene at low temperatures was carried out in a rapid compression machine over a wide range of temperatures, pressures and fuel/air equivalence ratios. Ignition delay times were measures at temperatures in the range 650–1000 K, at reflected shock pressures of 10, 30 and 50 atm and at equivalence ratios of 0.29, 0.48, 0.96 and 1.92. These ignition delay times were compared to complimentary high pressure shock tube experiments measured previously [9] and extended in the present work to 50 atm. These

comprehensive ignition results were used to discover trends in reactivity over the entire temperature range of approximately 800–1400 K.

It was found that an increase in reflected shock pressure resulted in shorter ignition delay times (higher reactivity) for all equivalence ratios investigated, which is typical of the influence of pressure on fuel reactivity. The effect of equivalence ratio for these fuel-*air* mixtures is as expected; fuel rich mixtures have shorter ignition delay times indicating higher reactivity than fuel lean mixtures throughout the range although at higher temperatures the reactivity begins to converge as noted in previous publications.

It was noted that *n*-propylbenzene does not show typical low temperature chemistry (namely NTC behavior) as observed from alkyl aromatics with longer side chains [6, 10]. The reasons behind this are linked to the resonantly stabilized benzylic radicals and to the short alkyl side chain.

The kinetic reaction model devised by Diévart and Dagaut [25] and modified previously [9, 21] was extended to include low temperature chemistry and used to successfully capture the lower temperature chemistry present in these experiments. Special attention in the mechanism improvements was given to $R\dot{O}_2$ isomerization reactions and $H\dot{O}_2$ elimination reactions involving the secondary benzylic site on n-propyl benzene to obtain good agreement with the present experimental results. Although the low temperature pathways included in the mechanism do not result in the actual NTC behavior with negative slope on an Arrhenius plot, the sensitivity and reaction path analysis highlighted the importance of these reactions in controlling the ignition delay times at low temperature.

The simulations performed using this improved model captured the experimental data reasonably well and as such validated the model for homogeneous ignition while the experimental data gave an insight into the trends in reactivity in terms of reflected shock pressure, temperature and equivalence ratio.

6. Acknowledgments

NUIG acknowledge the financial support of the Saudi Arabian Oil Company. The LLNL work was performed under the auspices of the US Department of Energy by Lawrence Livermore National Laboratory under Contract DE-AC52-07NA27344 and was supported by the US Department of Energy, Office of Vehicle Technologies (program manager Gurpreet Singh). Co-author H.N. acknowledges the financial support "Young Researcher Overseas Visits Program for Vitalizing Brain Circulation" from Japan Society of the Promotion for Science.

References

[1] J. H. Burgoyne, Proc. Royal Soc. A 161 (1937) 48–67.

[2] J. H. Burgoyne, Proc. Royal Soc. A 171 (1939) 421–433.

[3] J. H. Burgoyne, T. L. Tang, D. M. Newitt, Proc. Royal Soc. A 174 (1940) 379–393.

[4] J. H. Burgoyne, Proc. Royal Soc. A 174 (1940) 394–409.

[5] T. Litzinger, K. Brezinsky, I. Glassman, Combust. Sci. Techol. 50 (1986) 117–133.

[6] A. Roubaud, R.Minetti, L. R. Sochet, Combust. Flame 121 (2000) 535–541.

[7] P. Dagaut, A. Ristori, A. El Bakali, M. Cathonnet, Fuel 81 (2002) 173–184.

[8] S. Gudiyella, K. Brezinsky, Combust. Flame 159 (2012) 940–958.

[9] D. Darcy, C. J. Tobin, K. Yasunaga, J. M. Simmie, J. Würmel, T. Niass, O. Mathieu, S. S. Ahmed, C. K. Westbrook, H. J. Curran, Combust. Flame 159 (2012) 2219–2232.

[10] H. Nakamura, D. Darcy, M. Mehl, C. Tobin, W. K. Metcalfe, W. J. Pitz, C. K. Westbrook, H. J. Curran, Combust. Flame (2013) submitted.

[11] W. S. Affleck, A. Thomas, Proc. Inst. Mech. Eng. 183 (19681969) 365–385.

[12] L. Brett, J. MacNamara, P. Musch, J. M. Simmie, Combust. Flame 124 (2001) 326–329.

[13] D. Lee, S. Hochgreb, Combust. Flame 114 (1998) 531–545.

[14] D. Lee, S. Hochgreb, Int. J. Chem. Kinet. 30 (1998) 385–406.

[15] J. Würmel, J. M. Simmie, H. J. Curran, Int. J. Vehicle Design 44 (2007) 84–106.

[16] W. M. Haynes, CRC Handbook of Chemistry and Physics, CRC Press, 91st Edition, (2010) 6–110.

[17] C. Morley, GasEq, Version 0.76, http//www.gaseq.co.uk (2004).

[18] R. Mével, P. A. Boettcher, J. E. Shepherd, Chem. Phys. Lett. 531 (2012) 22–27.

[19] W. K. Metcalfe, S.M. Burke, S. S. Ahmed, H.J. Curran, Intl. J. Chem. Kinet. (2013) submitted.

[20] W. K. Metcalfe, S. Dooley, F. L. Dryer, Energy Fuels 25 (2011) 4915–4936.

[21] D. Darcy, M. Mehl, J. M. Simmie, J. Würmel, W. K. Metcalfe, C. K. Westbrook, W. J. Pitz, H. J. Curran, Proc. Comb. Inst. 34 (2013) 411–418.

[22] C. Cavallotti, D. Polino, A. Frassoldati, E. Ranzi, J. Phys. Chem. A. 116 (2012) 3313–3324.

[23] R. G. Butler, I. Glassman, Proc. Combust. Inst. 32 (2009) 395–402.

[24] K. Narayanaswamy, G. Blanquart, H. Pitsch, Combustion and Flame 157, (2010) 1879–1898.

[25] P. Diévart, P. Dagaut, Proc. Combust. Inst. 33 (2011) 209–216.

[26] M. Mehl, W. J. Pitz, C. K. Westbrook, K. Yasunaga, C. Conroy, H. J. Curran, Proc. Comb. Inst. 33 (2011) 201–208.

[27] Y. Murakami, T. Oguchi, K. Hashimoto, Y. Nosaka, J. Phys. Chem. A 113 (2009) 10652–10666.

[28] M. Altarawneh, B. Z. Dlugogorski, E.M. Kennedy, J. C. Mackie, Proc. Combust. Inst. 34 (2013) 315–323.

[29] E. R. Ritter, J. W. Bozzelli, Int. J. Chem. Kinet. 23 (1991) 767–778.

[30] T. H. Lay, J. W. Bozzelli, A.M. Dean, E.R. Ritter, J. Phys. Chem. 99 (1995) 14514–14527.

[31] CHEMKIN-PRO 15101, Reaction Design, San Diego (2010).

[32] G. Mittal, C. J. Sung, "Rapid Compression Machine (RCM) Database, http://www.mae.case.edu/facilities/cdl/projects/rapidcomp/rapiddatabase/h2co (2009).

[33] C. K. Westbrook, H. J. Curran, W. J. Pitz, J. F. Griffiths, C. Mohamed, S. K. Wo, Proc. Combust. Inst. 27 (1998) 371–378.

[34] C. K. Westbrook, Proc. Combust. Inst. 28 (2000) 1563–1577.

[35] J. D. DeSain, S. J. Klippenstein, J. A. Miller, C. A. Taatjes J. Phys. Chem. A 107(22) (2003) 4415–4427.